

A Buck-Boost Transformerless DC-DC Converter Based on IGBT Modules for Fast Charge of Electric Vehicles

Borislav Dimitrov^{1*}, Khaled Hayatleh², Steve Barker³, Gordana Collier⁴, Suleiman Sharkh⁵, Andrew Cruden⁶

^{1,2,3,4} Oxford Brookes University; bdimitrov@brookes.ac.uk; khayatleh@brookes.ac.uk; stevebarker@brookes.ac.uk; gordanacollier@brookes.ac.uk

^{5,6} Southampton University; S.M.Sharkh@soton.ac.uk, A.J.Crudon@soton.ac.uk

* Correspondence: bdimitrov@brookes.ac.uk; Tel.: +44 (0)1865 482962

Received: date; Accepted: date; Published: date

Abstract: A transformer-less Buck-Boost DC-DC converter in usage for the fast-charge of electric vehicles, based on powerful high-voltage IGBT (Isolated Gate Bipolar Transistor) modules is analyzed, designed and experimentally verified. The main advantages of this topology are: simple structure on the converter's power stage; a wide range of the output voltage, capable to support nowadays vehicles on-board battery packs; efficiency and power density accepted to be high enough for such class of hard-switched converters. A precise estimation of the loss, dissipated in the converter's basic modes of operation – Buck, Boost, and Buck-Boost is presented. The analysis shows an approach of loss minimization, based on switching frequency reduction during the Buck-Boost operation mode. Such a technique guarantees stable thermal characteristics during the entire operation, i.e. battery charge cycle. As the Buck-Boost mode takes place when Buck and Boost modes cannot support the output voltage, operating as a combination of them, it can be considered as critically dependent on the characteristics of the semiconductors. With this, the necessary duty cycle and voltage range, determined with respect to the input-output voltages and power losses, require additional study to be conducted. Additionally, the tolerance of the applied switching frequencies for the most versatile silicon-based powerful IGBT modules is analyzed and experimentally verified. Finally, several important characteristics, such as transients during switch-on and switch-off, IGBTs voltage tails, critical duty cycles, etc., are depicted experimentally with oscillograms, obtained by an experimental model.

Keywords: Buck-Boost, DC-DC, converter, fast battery charger, electric vehicles

1. Introduction

The technology of fast charge is an inevitable part of a future transport system based on electric vehicles, had been proven by numerous studies [1-4]. Fast can be considered a charge cycle of 20 min to 40 min., during which the vehicle battery reaches 80% of its capacity. For this purpose, a significant amount of energy must be transferred from the source, which can be the electrical grid or stand-alone renewable energy source, etc. to the car battery. The equipment necessary for that purpose is a powerful electronic converter working as a battery charger.

Nowadays, the leading fast charger schematics are based on different advanced switched-mode power supply topologies: LLC resonant converters with soft switching [5, 6], phase-shift converters [7], two and three-level, three-phase, full-bridge DC-DC converters [8, 9], bi-directional vehicle-to-grid converters [10], etc. These are advanced switch-mode converters which have significant technical advantages and respectively considerable areas of application. Their disadvantages are complexity, a high number of switches, high switching frequencies and therefore EMI (electromagnetic interference) problems, a complex control system, high price, difficulties with manufacturability, etc. Such problems can be avoided with a simple Buck-Boost structure based on IGBT modules.

The aim of this research is a powerful Buck-Boost transformerless converter, based on a small number of IGBT modules to be analyzed and experimentally verified. Such a solution has the potential to be used as a powerful (150 kW) battery charging system based on a budget-friendly topology with high power density and efficiency. These requirements are feasible due to the simple structure, which this type of DC-DC converter usually had. Inherently, their power stages are based on a small number of semiconductors. In this case, an application of the currently available powerful silicon-based IGBTs would allow for only two modules to be used.

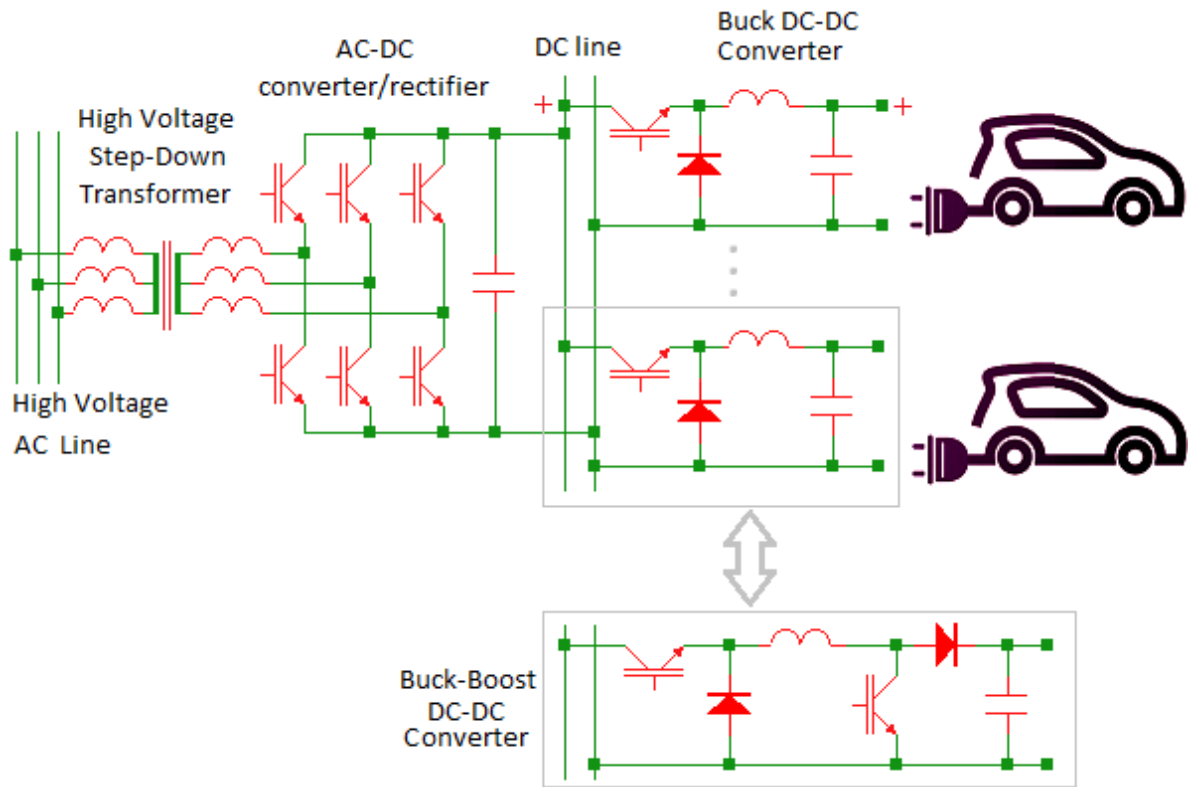


Figure 1. A fast-charge station with main elements DC-DC Buck converters, low frequency transformer; AC-DC converter-rectifier with PFC and filter. The designed Buck-Boost converter is shown as a suggestion to replace the Buck converters.

Figure 1 shows the power part of transformerless fast-chargers based on Buck topology which is widely used today. Such charging stations are powered by a high-voltage distribution system through a low-frequency power transformer in order for their impact over the low-voltage system to be minimized. As a rectifier is usually used a controllable AC-DC converter with PFC (Power Factor Correction). The analyzed and experimentally verified Buck-Boost converter based on powerful IGBT modules is designed to replace the Buck converters, as fig. 1 shows. The major benefit of a Buck-Boost converter topology is the inherent ability the output voltage to be lower or bigger than the input DC voltage. Such characteristic would guarantee the flexibility of the charging system and its applications in the wide range of the growing battery pack voltages.

The Safe Operation Area (SOA), as one of the most important features, strongly depends on switching and conducting losses in a switch-mode application, and respectively the accumulated junction temperature. In [11] a study dedicated to over-current and over-temperature breakdown for high-voltage, high-current IGBT modules is presented. It is shown through simulations and experimental verification, that breakdowns can happen when the modules operate in restrictive temperature environments. Although the paper is focused mainly on railway inverters, the presented analysis is supposed to be actual for DC-DC Buck-Boost converters as well. The same research gives information, according to which the maximum overloading, therefore the probable failure, occurs mostly when high current and high voltage are simultaneously applied across the device during the switch-on or switch-off periods. Additionally, the dependency of IGBTs dynamic

characteristic on the temperature can be verified with modeling and simulations [12, 13, 14]. The proposed models have application in converter design, mode-of-operation analysis, lifespan estimation, analysis and design of the necessary cooling system, etc.

A study of fast-charging under extreme temperature conditions is presented in [15]. This paper presents power quality performance, addressing important characteristics as ambient temperature range and its influence over the Total Harmonic Distortion (THD), power factor, etc. Although this research is not focused on such issues, the concluded temperature range ($+40^{\circ}\text{C} \div -15^{\circ}\text{C}$) and the considerations given for low THD are taken into account in this analysis.

Thermal modes of operation of IGBT modules are shown with modeling and simulation in [16, 17]. The presented numerical analysis gives fundamental information about temperature dissipation and thermal field distribution in the modules. As the results are not focused on a specific converter, but rather than more broad study is offered, they are applicable for a Buck-Boost converter in Buck, Boost and Buck-Boost modes of operation.

Two different IGBT structures, Floating Island (FLI) and Revers Conducting (RC-IGBT), are analyzed in [18] and [19, 20] respectively. These technologies offer significant advantages such as a lower break-down voltage, which leads to lower losses and better efficiency, better robustness under fault conditions, etc. In [20] an application in high voltage railway converters is presented. A significant decrease in losses, accomplished with RC-IGBT modules compared to conventional IGBT modules is shown. Such efficiency improvements can also be expected to be achieved for battery charge applications based on the proposed topology, although the published literature in this direction is insufficient.

Potentially, Buck-Boost DC-DC transformerless converters can face short-circuit failure modes under certain conditions. Sources [21-26] offer significant information in this direction as follows: IGBT structural behavior under short-circuit [21]; breakdown and thermal runaway mechanisms leading to destructive failure [22]; damages from electrostatic discharge [23]; IGBTs mechanical stress under short-circuit conditions [24]; turn-off failure mechanism [25]; robustness of IGBT modules during turn-off commutation.

In [25] experimentally obtained oscillograms are given, which clearly show the mechanism of turn-off failure of an IGBT module. The depicted problem with overcurrent leading to a thermal runaway and avalanche breakdown supposed to be actual for DC-DC Buck-Boost converters, especially in the border between Buck and Boost modes of operation. The same suggestions can be confirmed from the experimental data presented in [26].

The literature research showed that the Buck-Boost topology is used for low-voltage converters, based on MOSFETs, completed by four transistors with synchronous switching [27-37]. Despite that, its application with high-voltage IGBTs, which considering the different voltage ranges and transistors' parameters, requires the analysis and design procedure to be altered. The proposed application requires study to be undertaken in several directions: a possible range of the switching frequencies at the Buck-Boost mode of operation for converter based on high-voltage and high-current IGBT modules; thermal mode of operation and possibilities for the dissipated losses and temperature, to be reduced; the possible voltage ranges between the three modes of operation Buck, Boost and Buck-Boost to be analyzed and experimentally verified. Additionally, the low-voltage MOSFET converters are implemented with control systems based on Application-Specific Integrated Circuits (ASICs), directly powered by the low input voltage [38-41] usually in a range 24-60V, which is inapplicable for high-voltage IGBT applications up to 1000V. In this sense, the novelty in the current research consists in the application of high-voltage, high-power IGBT modules, half-bridge or integrated transistor-diode structures, applied for vehicles fast charge converters, which cannot be completed with the presented low-voltage applications. Such a technology needs further development in two directions:

- The suggested Buck-Boost converter maintains three modes of operation: Buck, Boost, and Buck-Boost. The third one applies on the border between Buck and Boost, as in this condition neither of them can support the output voltage. In [27, 28, 29] it is correctly suggested that the implementation of Buck-Boost mode has the potential to decrease the losses and to increase the efficiency of the DC-DC power stage. For this class of hard-switched converters the targeted

efficiency can be set at 97-98% for both semiconductors. In the currently available literature, the IGBT operation at Buck-Boost operation mode is not presented in details, considering the relatively low switching frequency (8kHz – 16kHz), significant voltage tails for the silicon based IGBTs, and the necessary time rages.

- The voltage region of the Buck-Boost operation mode is of primary importance for achieving a robust and efficient operation [35, 36, 37]. Several techniques are applicable mainly used for MOSFET based DC-DC converters: active inductor balancing for interleaving Buck-Boost converters [35], reduction of the passive elements [36], high level of implementation of a digital control system for low power portable electronics. It depends on the semiconductors' parameters, or in this case, currents and voltage tails of the selected IGBT modules, the maximum duty cycle at Buck and Boost modes, and switching frequency, etc. Its importance requires it to be analyzed and verified experimentally.

The paper is organized as follows: chapter two presents an analysis of the proposed converter, which is limited to the power stage of the Buck and Boost parts; chapter three shows an experimental study, conducted with an experimental model; conclusions are summarized in chapter four.

2. Analysis of the proposed converter

Figure 2 shows the proposed Buck-Boost converter for fast battery charge, derived from the basic circuit, shown in figure 1. The input power supply consists of a low-frequency three-phase isolation transformer Tr1, connected to low-voltage grid (0.4 kV), as in this case a high-voltage system has not been available. The voltage after rectification and filtering is 660 V, assumed to be stable on the input side of the DC-DC converter. As this part of the circuit is not the object of this research it has been simplified for experimental purposes only.

The Buck-Boost converter consists of two IGBT modules, M1 and M2, with transistor-diode structure Q1- D1 and Q2- D2, inductor L1, input C1 and output C2 capacitors, and snubber capacitors C3 and C4. The output voltage can vary in the range of 300V – 1000V, depending on the vehicle battery (B1) type and state of charge (SoC). The transistor-diode modules, shown in figure 2, are particularly designed for such type converters.

The transistor-diode modules, shown in figure 2, are particularly designed for such type converters. Alternatively, half-bridge modules (figure 3) can be used. Although additional control signals are necessary for transistors Q2 and Q3, for most of the modules only their reverse diodes can be used for simplification. Table 1 (Appendix A) shows some currently available IGBT modules, rated at the required power, offered by several manufacturers.

As it was mentioned above, a typical feature of these type of converters are the three modes of operation. First, the Buck mode when $V_{out} < V_{in}$, or in this analysis, a range 300V – 600V is assumed (figure 4). During Buck mode, the transistor Q1 is controlled by Pulse Width Modulation (PWM) and transistor Q2 is permanently OFF. Module M1 dissipates switching and conductive losses, while only the diode from M2 has conductive losses.

The Boost operation mode is applicable when $V_{out} > V_{in}$, or here a range 700V – 1000V V_{out} is assumed. During Boost mode, the transistor Q2 is under PWM control and transistor Q1 is permanently ON. Vice versa on the previous mode, M2 dissipates switching and conductive losses, while M1 only has conductive losses. Diode D1, module M1, is permanently OFF and can be accepted as excluded from the analysis.

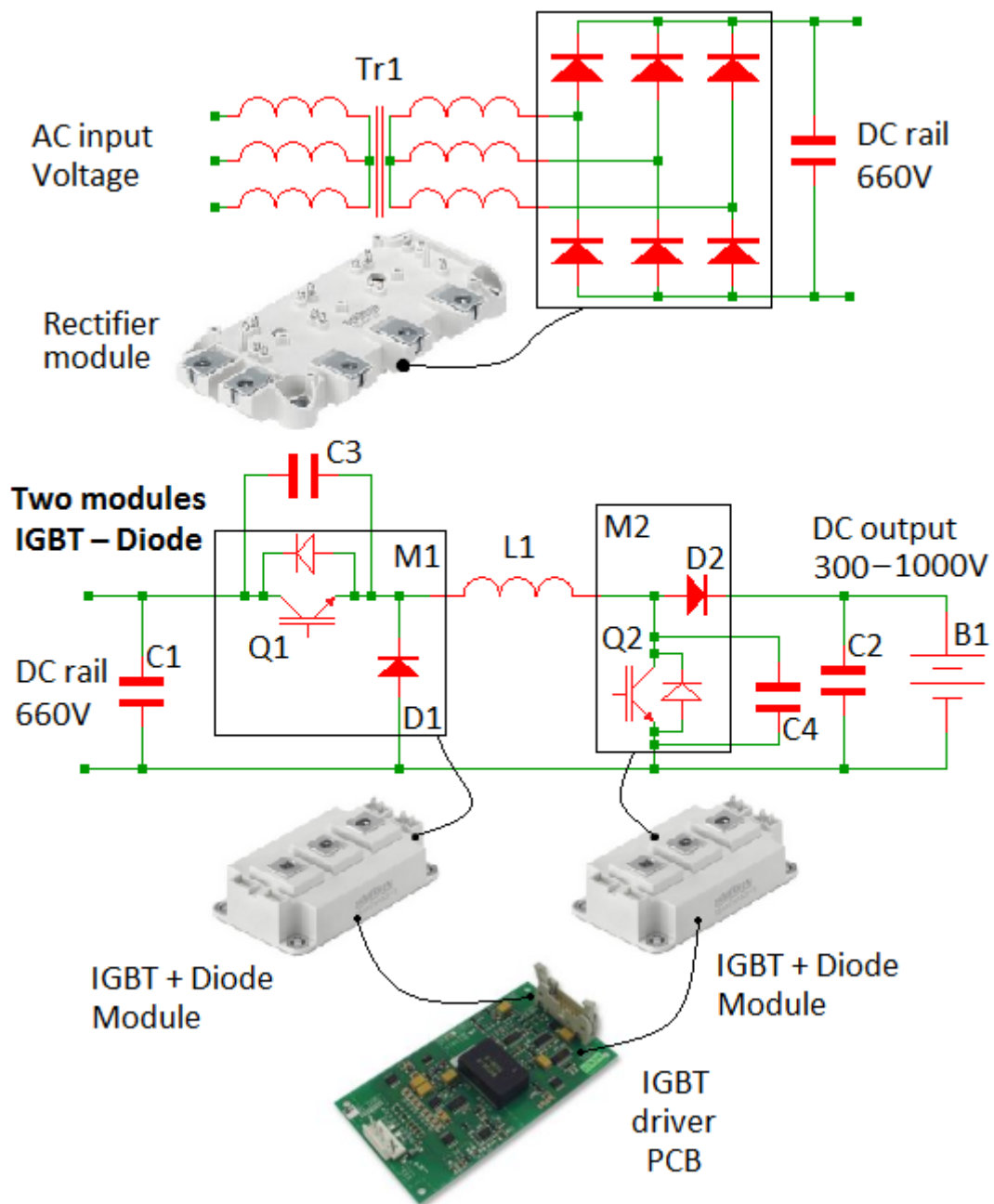


Figure 2. The proposed Buck-Boost converter for fast charge, based on IGBT modules (see Table 1 Appendix).

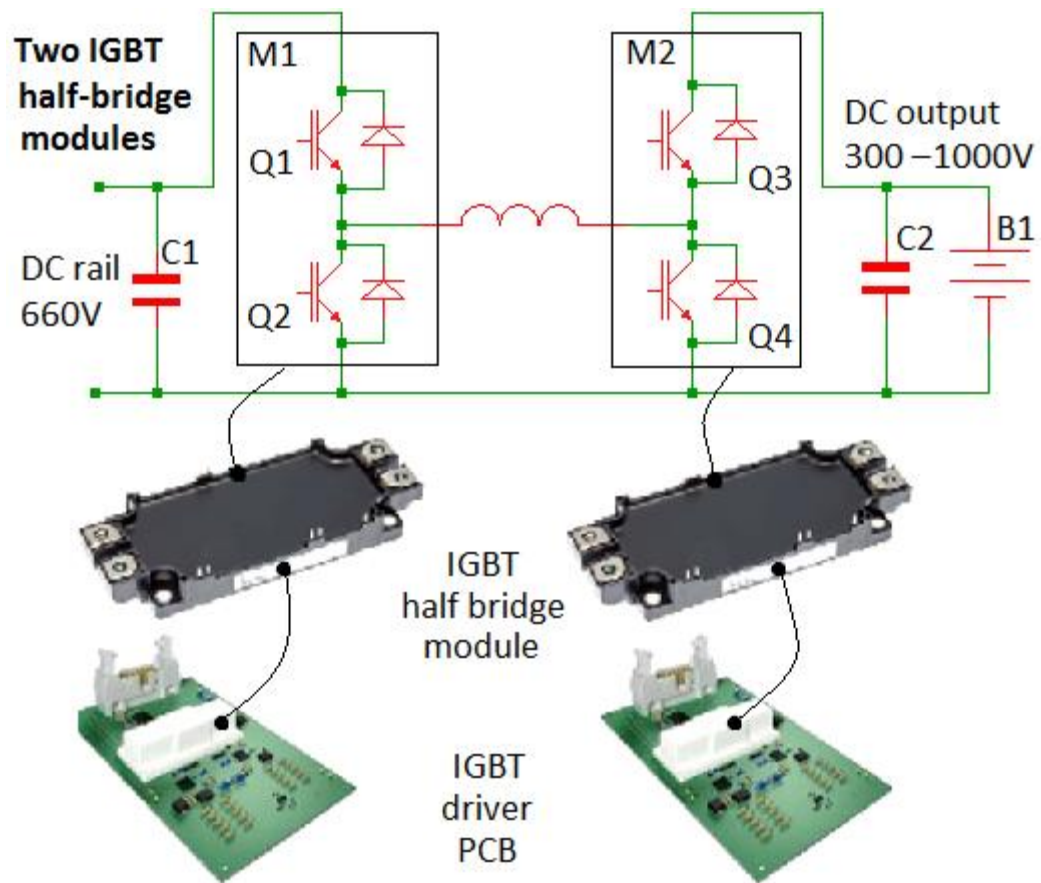


Figure 3. Buck-Boost converter, based on half-bridge IGBT modules with drivers (see Table 1 Appendix).

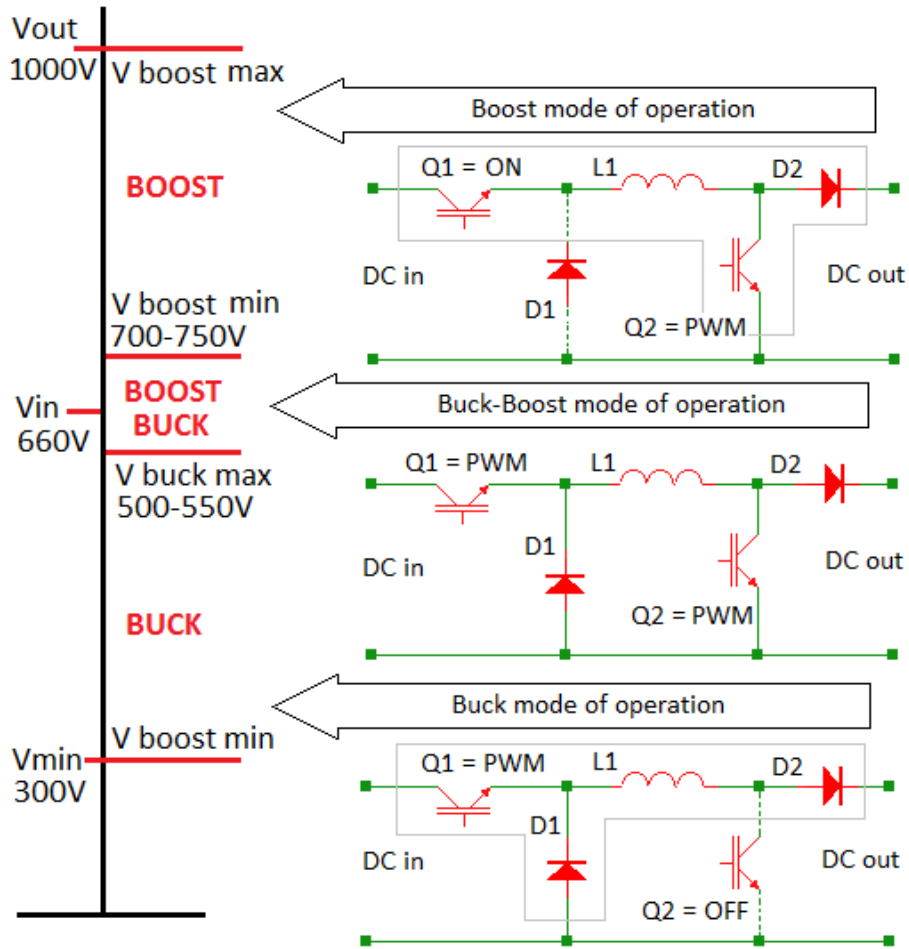


Figure 4. Buck, Boost and Buck-Boost modes of operations. Their activation and the necessary Pulse Width Modulation (PWM) is presented according to the output voltage range.

The Buck-Boost mode is necessary when V_{out} and V_{in} are approximately equal and neither of previous modes can support the normal operation. The problem occurs due to the duty cycle, which under equalization between V_{out} and V_{in} will be too high during Buck mode or too low during Boost mode of operation. Here, considering the input DC voltage of 660V, a flexible range of $V_{out} > 550V - 600V$ and $V_{out} < 700V - 750V$ is assumed, as figure 4 shows. In this mode IGBT module M1 operates as a Buck converter with a fixed duty cycle, between 0.7 – 0.8 and IGBT module M2 operates as a Boost converter with variable duty cycle 0.1 – 0.4 (figure 5). The presented PWM signals are produced by a flexible control system based on microcontroller, current and voltage measurement galvanically isolated circuits, shown in the same figure. These ranges are considered from manufacturers' documentation [38-41], where they are recommended only for MOSFETs based converter and should be checked for IGBTs. Another factor, which has a significant impact on the duty cycle restriction, is imposed from the snubber capacitors C3 and C4, figure 2. As for the IGBT modules, due to their relatively low switched frequency and high voltages, they can reach 1.5 μ F – 2 μ F, i.e. much bigger than MOSFET based applications, and therefore their effect over the operation modes must be verified experimentally.

Under the suggested sequence of modulation Buck, Buck-Boost and Boost, a smooth output voltage must be assured during the entire charging cycle, regardless of its stage – constant current or

constant voltage. Eventually, the output current given in fig. 5 shows that the Buck, Boost, and Buck-Boost are continuous modes of operation.

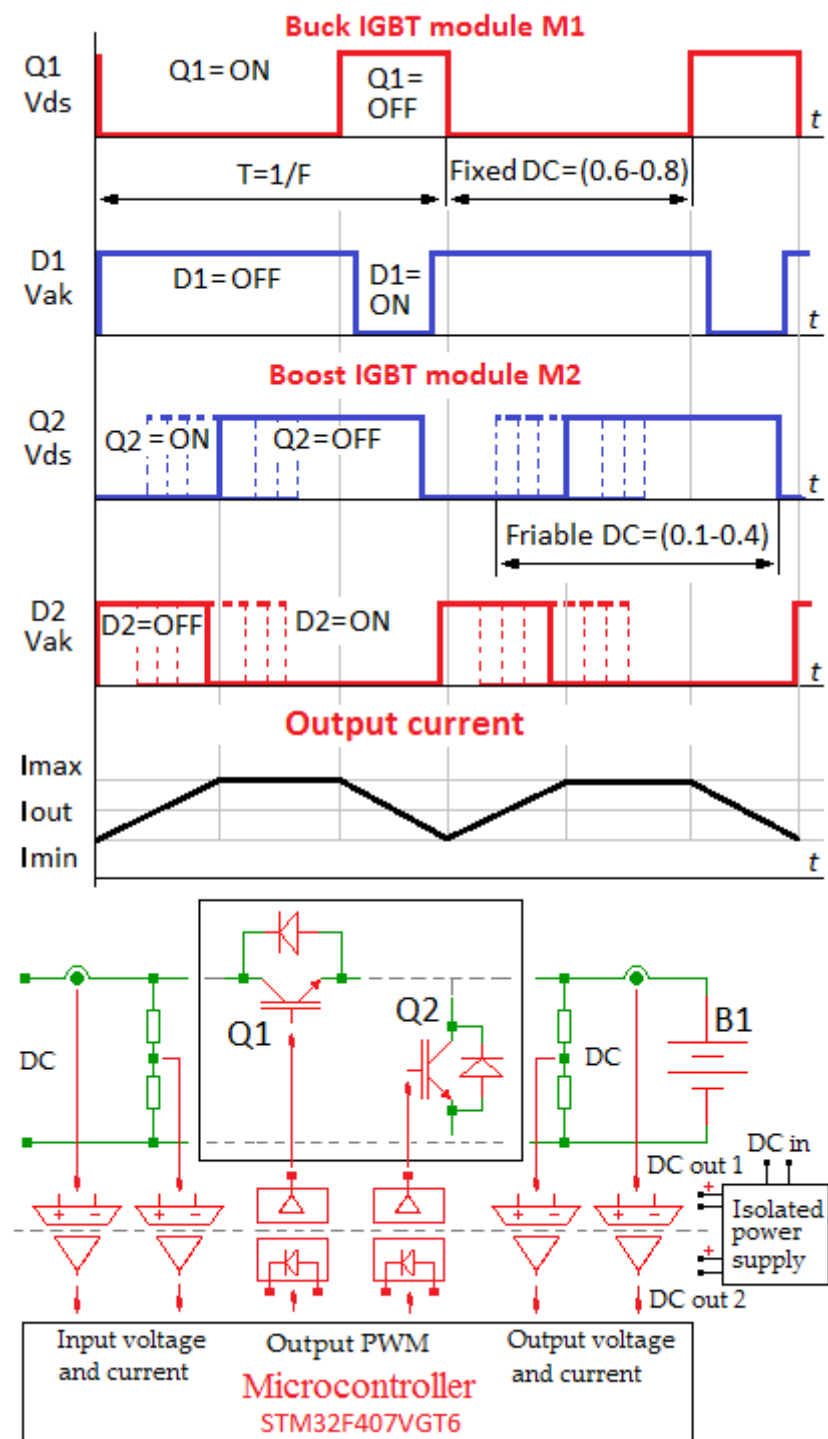


Figure 5. Buck-Boost mode of operation and block diagram of the control system.

205

Table 2. Buck and Boost mode of operations.

206

D is the duty cycle; V_{out} is the output voltage; V_{in} is the input voltage; T is the period (sec); t_{on} is the ON time (sec); F_{sw} is the switching frequency (Hz); L is the inductance (H); $I_{max out}$ is the maximum output current.

207

208

| Buck | | Boost |
|--|-----|---|
| Duty Cycle | | |
| $D_{Buck} = \frac{V_{out}}{V_{in}} = \frac{t_{on}}{T}$ | (1) | $D_{Boost} = 1 - \frac{V_{in(min)}}{V_{out}}$ (2) |
| Inductor | | |
| $L_{Buck} = \frac{V_{out}(1-D)}{F_{sw} \times \Delta I_L}$ | (3) | $L_{Boost} = \frac{V_{IN(min)} \times D_{boost}}{F_{sw} \times \Delta I_L}$ (4) |
| Maximum output current | | |
| $I_{max out Buck} = I_L - \frac{\Delta I_L}{2}$ | (5) | $I_{max out Boost} = \left(I_{L(min)} \frac{\Delta I_L}{2} \right) \times (1 - D)$ (6) |
| Maximum switching current | | |
| $I_{sw max Buck} = \frac{\Delta I_{max}}{2} + I_{out}$ | (7) | $I_{sw max Boost} = \frac{\Delta I_{max}}{2} + \frac{I_{out}}{1 - D_{boost}}$ (8) |

209

During Buck-Boost mode, modules M1 and M2 operate with PWM at the same time, dissipating switching and conductive losses. Such operation has the potential to heat the converter to a dangerous temperature level, i.e. the above presented problem. Improving the cooling system is not always a universal solution, because it would have a negative impact on power density and overall efficiency [39, 40]. Hence, other techniques for minimizing the losses must be implemented. The suggested approach in this research is the switching frequency to be reduced during Buck-Boost mode, and the necessary parameters of such reduction must be analyzed and verified [41].

210

As Buck and Boost mode of operations have trivial descriptions [42, 43], although fundamental for this converter, their basic equations are given in Table 2 without further explanation.

211

The Buck-Boost mode of operation can be derived from Buck and Boost modes, as in this mode, both operations are cascaded. If the voltage after the Buck part of the converter is derived from equation (1) as [38]:

212

$$V_{out buck} = D_{buck} \times V_{in}, \quad (9)$$

213

and the output voltage, i.e. after the Boost part, is based on Boost duty cycle (2) as:

214

$$V_{out} = D_{boost} \times V_{out buck}, \quad (10)$$

215

then the Buck-Boost mode of operation can be written as:

216

$$\frac{V_{out}}{V_{in}} = D_{buck} \times D_{boost}, \quad (11)$$

217

leading to [38]:

218

$$\frac{V_{out}}{V_{in}} = \frac{D_{buck}}{1 - D_{boost}}. \quad (12)$$

The losses estimation is based on the following requirements:

- The converter must be designed to work with constant output current and constant output voltage. The voltage range is shown in figure 3 as $V_{out.min} = 300V$, $V_{out.max} = 1000V$. The accepted current range for this design is $I_{out.nom} = 150A$, $I_{out.peak} = 200A$. With that, the converter must be able to work appropriately, i.e. on the required efficiency and thermal equilibrium, under the nominal output power of $P_{out.nom} = 150kW$ and peak power of $P_{out.peak} = 200kW$.
- Usually, the targeted efficiency for this class of transformerless, hard-switched converters is within the range 96-97%, and should not be smaller than 95% at any modes of operation. In this paper, the efficiency is estimated only for both modules M1 and M2 (figure 2), as they are the major focus of this research. This means, the efficiency should be over 98% at the nominal current of 150A, and over 97% at maximum current of 200A, which gives enough energy budget for the final efficiency target of the entire converter to be achieved.
- The nominal switching frequency is 12kHz for the Buck and Boost operation modes but it can be reduced to 10kHz in order the expected losses under Buck-Boost mode to be minimized. The output voltage ripples should be no bigger than 20% in any mode of operation. Although some of the analyzed modules given in Table 1 (Appendix) are rated at higher than 20kHz frequencies, which has the potential to reduce the size of the inductor and output capacitors, this research has found that such switching frequencies are not feasible at the required power level for hard-switching topology.

The energy analysis is based on fundamental equations and dependencies for IGBT transistors, presented in the literature sources [44-48]. Because of that, in this case, the necessary mathematical apparat is simplified to the usage of basic equations for losses calculation and IGBT characteristics from manufacturers' datasheets [49-53].

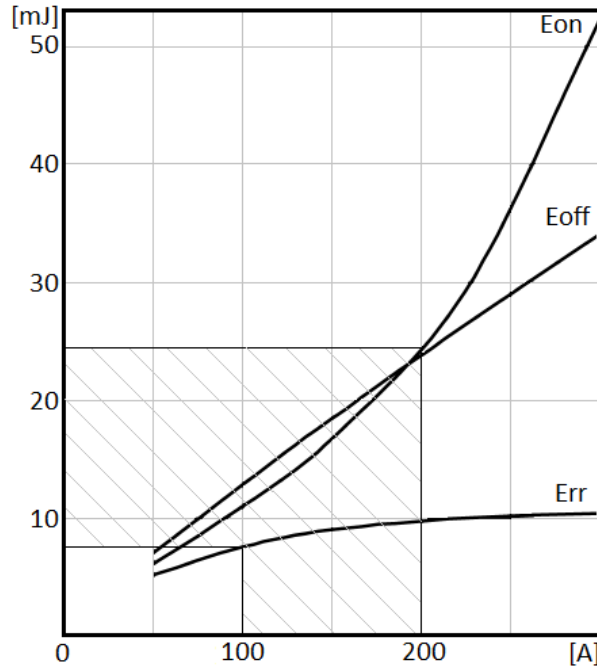


Figure 6. Accumulated energies E_{ON} , E_{off} , E_{rr} .

The total losses of an IGBT are given as a sum of two components – conduction P_{cond} and switching P_{sw} losses, given by the equation [46, 47, 48]:

$$P_{loss\ IGBT} = P_{cond} + P_{sw} \quad (13)$$

As the switching losses are sum of turn ON and turn OFF losses, or

$$P_{sw} = P_{turn\ ON} + P_{turn\ OFF}, \quad (14)$$

can be written:

$$P_{loss\ IGBT} = P_{cond} + P_{turn\ ON} + P_{turn\ OFF} \quad (15)$$

The conductive losses are calculated according to the current and the semiconductor resistance R_{on} , or:

$$P_{cond} = I_{RMS}^2 \times R_{on} \quad (16)$$

The switching losses are calculated from the accumulated energies during the transient switched ON E_{ON} , switched OFF E_{off} , reverse recovery E_{rr} , and switched frequency f_{sw} , given from the equation [46, 47, 48]:

$$P_{sw} = (E_{ON} + E_{off} + E_{rr}) \times f_{sw} \quad (17)$$

The necessary E_{ON} , E_{off} , E_{rr} are can be obtained as functional current dependencies at given gate drive resistance, as it is shown in figure 6 as an example. As for the suggested battery charger, the output current must vary in the wide area $I_{min} = 100A - I_{nom} = 150A - I_{max} = 200A$, the necessary energies are in a range of several tents mJ, shown in the dashed area in the same pictures.

The temperature on the junction can be found from the dissipated power, calculated from equation (15), thermal resistance R_{th} , and the ambient temperature T_a as follows [46, 47, 48]:

$$T_j = (P_{loss\ IGBT} \times R_{th}) + T_a \quad (18)$$

The thermal resistance is given as:

$$P_{th} = R_{th\ j-c} + R_{th\ c-hs} + R_{th\ hs-a} \quad (19)$$

where $R_{th\ j-c}$ is the thermal resistance junction to case; $R_{th\ c-hs}$ is the thermal resistance case to heatsink; $R_{th\ hs-a}$ is the thermal resistance heatsink to ambient.

Figure 7 shows in details the power losses and overall efficiency at the DC-DC stage of the converter during Buck mode, at switching frequency 12kHz. The graphics are given as follows: 1 – DC-DC power stage losses, dissipated from both modules M1 and M2; 2 – switching and conductive losses from the IGBT transistor Q1, module M1; 3 – losses from the diode D1, module M1; 4 – losses from the diode D2, module M2; 5 – overall efficiency of the power stage of the converter, calculated over the modules M1 and M2. As the obtained data shows, the overall efficiency does not drop under 98% at 150A nominal current and 1000W losses.

The same data, as a functional dependence of the duty cycle (DC), is presented in figure 8. Graphic 1 shows linear losses increase with the DC increase, which increases the IGBT junction temperature. With a maximum junction temperature of 175°C for silicon-based IGBTs and 15% safety margin, a temperature of 150°C can be accepted as a maximum possible. In this analysis a constant surface temperature of 40°C is accepted, which have to be supported by the cooling system. The data shows that it is reached, depending on the IGBT characteristics, in the duty cycle range between 0.8-0.9, which must be the maximum duty cycle for Buck mode. On the other hand, the

output voltage from the Buck mode, calculated with this duty cycle range and the accepted input voltage of 660V, gives approximately the voltage range of 550V – 600V as this is suggested at the beginning in figure 4. The results explicitly show that such frequency reduction must be applied at the end of the Buck mode, entire Buck-Boost mode and the beginning of the Boost mode.

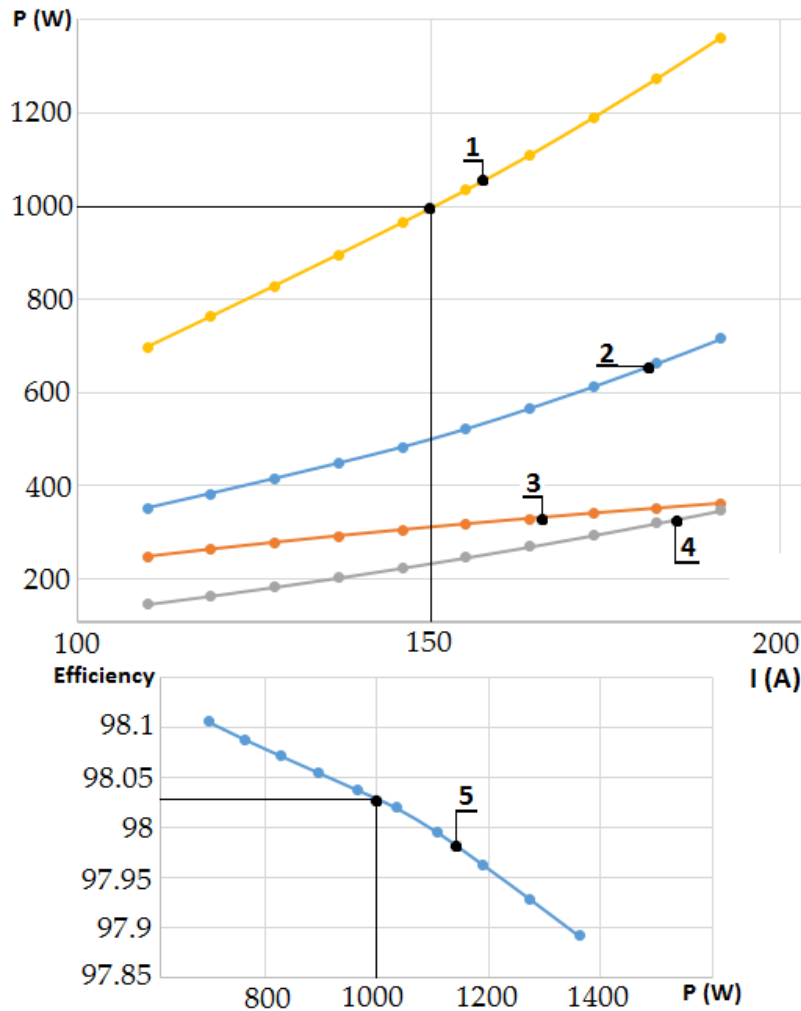


Figure 7. Buck Mode of operation. 1 – DC-DC power stage losses; 2 – Buck transistor Q1 losses (IGBT module M1); 3 – Buck diode D1 losses (IGBT module M1); 4 – Boost diode D2 losses (Boost module M2);

The magnitude of the frequency reduction approach to decrease the junction temperature, hence losses on the power stage, is shown in figure 8, graphic 4. A rapid temperature drop occurs at the moment of switching frequency reduction from 12kHz to 10kHz. This also means, that the cooling system, air or water cooled heat sink, should be designed for the lower power dissipation without need of oversizing.

Similarly, the losses for Boost operation mode are shown in figure 9 as follows: 1 – losses, dissipated from the DC-DC power stage, which includes Buck M1 and Boost M2 modules; 2 – Boost transistor Q2, commutated with PWM, module M2; 3 – Boost diode D2, installed in the same module; 4 – conductive losses dissipated by the buck transistor, as it is permanently switched ON; 5 – the efficiency is slightly slower than the expected 98%, but in the range of the acceptable error. Additionally, a comparison between Buck (figure 6) and Boost (figure 8) operation modes shows that their energy characteristics are similar at the same switching frequency.

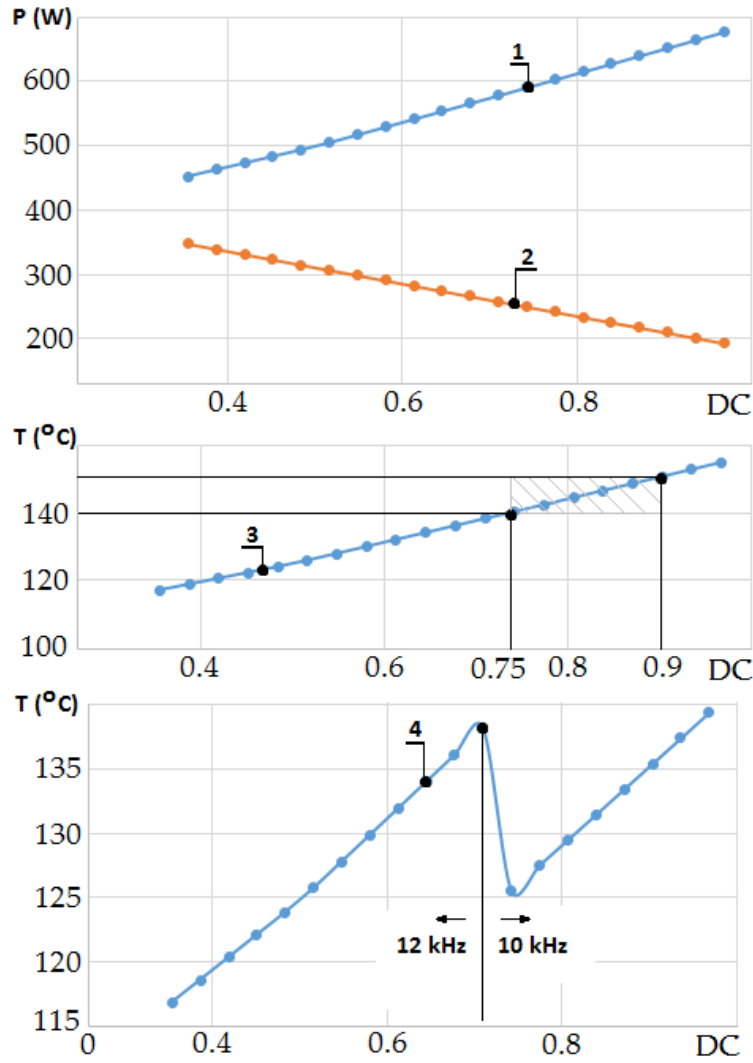


Figure 8. Buck mode of operation. 1. Buck transistor losses; 2. Buck diode losses; 3. Buck module temperature. 4. Reduction of the switching frequency from 12kHz to 10 kHz.

Power losses at Buck-Boost operation mode are shown in figure 10. Graphic 1 shows the dissipated losses at 12kHz, which are approximately 300W – 350W more for the entire current range than the losses at reduced to 10kHz switching frequency (graphic 2). Furthermore, graphic 2 correlates with graphic 1 (figure 7, Buck mode) and graphic 1 (figure 9, Boost mode), which suggests the same losses level for the entire output voltage and current regions, shown in figure 4.

The output design parameters are given in table 3. The output current ripple is calculated for the assumed output voltage range of 300V – 1000V, at 150A output nominal current, and 660V input voltage. The inductor L1 (figure 2) is 500μH, which is an acceptable value for low-frequency DC-DC transformerless converters. The result shows that output voltage ripple of under 20% is achievable for the three modes of operation with the suggested frequency reduction.

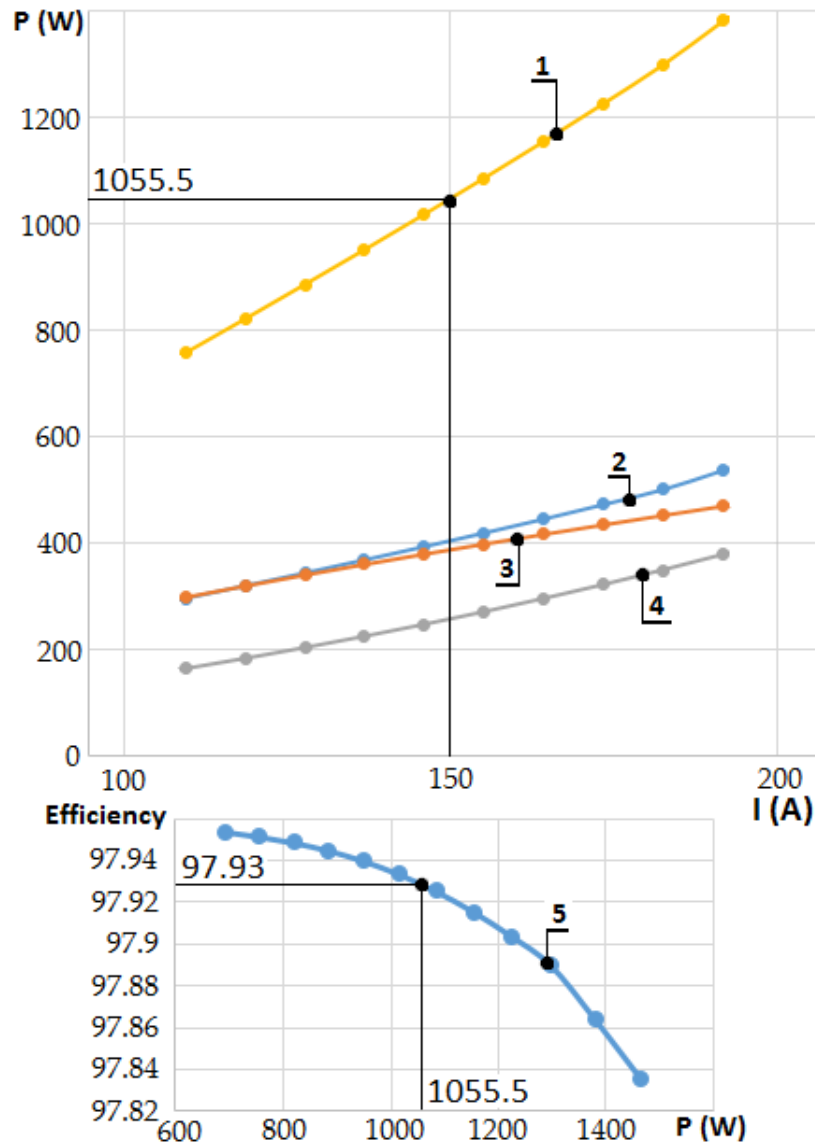


Figure 9. Boost mode of operation. 1 – DC-DC power stage losses; 2 – Boost transistor Q2 switching and conductive losses (IGBT module M1); 3 – Boost diode D2 losses (IGBT module M1); 4 – Buck transistor Q1 losses, permanently switched ON (IGBT module M2); 5 – Efficiency.

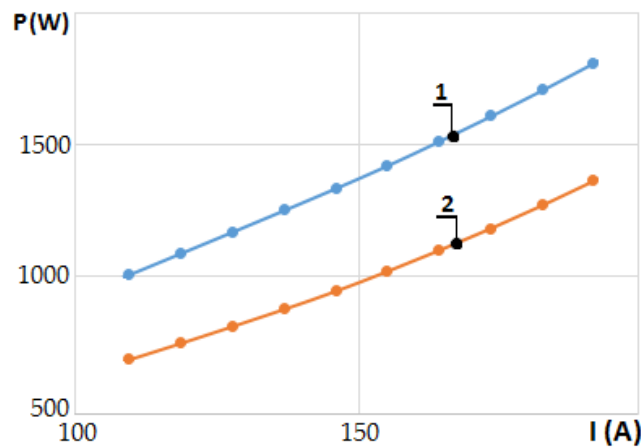


Figure 10. Buck-Boost operation mode power losses compensation with switching frequency reduction. 1 – losses at 12 kHz switching frequency; 2 – losses at 10 kHz switching frequency.

Table 3. Buck-Boost converter time parameters.

| Output voltage to the charged battery (V) | Switching frequency (kHz) / Period (μs) | Duty cycle | On-Time (μs) | Off-Time (μs) | Output current ripple (A) / (%) |
|---|---|------------|--------------|---------------|---------------------------------|
| Buck mode of operation (Buck module M1) | | | | | |
| 300 | 12/83.33 | 0.45 | 37.93 | 45.41 | 27.31/18.2 |
| 350 | 12/83.33 | 0.53 | 44.23 | 39.1 | 27.42/18.28 |
| 400 | 12/83.33 | 0.61 | 50.54 | 32.79 | 26.28/17.52 |
| 450 | 12/83.33 | 0.68 | 56.85 | 26.49 | 23.88/15.92 |
| Buck – Boost mode of operation (Buck module M1; the output voltages given for this mode of operation are after Buck module M1) | | | | | |
| 500 | 10/100 | 0.76 | 75.78 | 24.22 | 24.25/16.17 |
| 525 | 10/100 | 0.79 | 79.57 | 20.43 | 21.48/14.32 |
| 550 | 10/100 | 0.83 | 83.35 | 16.65 | 18.34/12.22 |
| Buck – Boost mode of operation (Boost module M2; the output voltages given for this mode of operation are at the output of the converter) | | | | | |
| 600 | 10/100 | 0.17 | 16.76 | 83.24 | 16.76/9.3 |
| 650 | 10/100 | 0.19 | 19.32 | 80.68 | 20.28/10.91 |
| 700 | 10/100 | 0.22 | 21.51 | 78.49 | 23.66/12.38 |
| Boost mode of operation (Boost module M2) | | | | | |
| 750 | 12/83.33 | 0.12 | 10.07 | 73.26 | 13.29/7.79 |
| 800 | 12/83.33 | 0.17 | 14.64 | 68.69 | 19.33/10.62 |
| 850 | 12/83.33 | 0.22 | 18.68 | 64.65 | 24.66/12.75 |
| 900 | 12/83.33 | 0.27 | 22.27 | 61.06 | 29.4/14.36 |
| 950 | 12/83.33 | 0.31 | 25.48 | 57.85 | 33.64/15.57 |
| 1000 | 12/83.33 | 0.34 | 28.37 | 54.96 | 37.45/16.47 |

335 As this research is to offers more broad study, the presented data in figures 6, 7, 8, 9 and table 3 is
336 average. It has been calculated from IGBT modules datasheets, given in table 1 (Appendix A), using
337 their basic parameters and the above presented equations (1-19). However, the interested reader
338 could use specific IGBT modules for a more precise design of a Buck-Boost converter used as a
339 battery charger or other applications. In this case, the received results would differ from the
340 presented data in a small acceptable range.

341 **3. Experimental data.**

342 The experimentally obtained oscillograms depict the most important voltages and currents
343 waveforms for the Buck, Boost, and Buck-Boost mode of operation as follows:

- Figure 11. Graphic 1 shows the drain-to-source voltage of transistor Q1, without a snubber capacitor. The experiment is conducted at nominal characteristics – switching frequency of 10kHz – 12kHz, nominal current 150A, output voltage within the suggested in figure 4 range of 300V – 550V, input voltage of 660V. In this mode, the voltage peak during the switch-off period, shown in the same figure, cannot exceed the maximum rated IGBT voltage, but can make the entire system unreliable. Graphic 2 shows the current through the transistor Q1.
- Figure 12. The same characteristics are shown with a snubber capacitor of 470nF, 2kV added in parallel to Q1. The design of this capacitor is out of the scope of this paper, but its experimental verification clearly shows its impact over the switched-off time. This oscillogram shows that the converter operates without overvoltages during the transient proves, but due to the capacitor included dv/dt is lower, which has negative impact on the switching losses. Hence, the converter ability to sustain the output voltage during this mode at duty cycle higher than 0.85 – 0.9 can be compromised.
- Figure 13. With a duty cycle over 0.95 the IGBT module practically cannot be fully switched-off, i.e. the current is not stably established at zero ampere, which can cause unacceptable losses and overheat. This result complies with the analytical obtained result, presented above, showing that the duty cycle should be limited to 0.87-0.85 for a converter based on IGBT modules.
- Figure 14. The current through the inductor during the Buck mode of operation is presented. Graphic 1 shows the current through Q1 and graphic 2 the current through the diode D1, during the OFF time of the transistor Q1

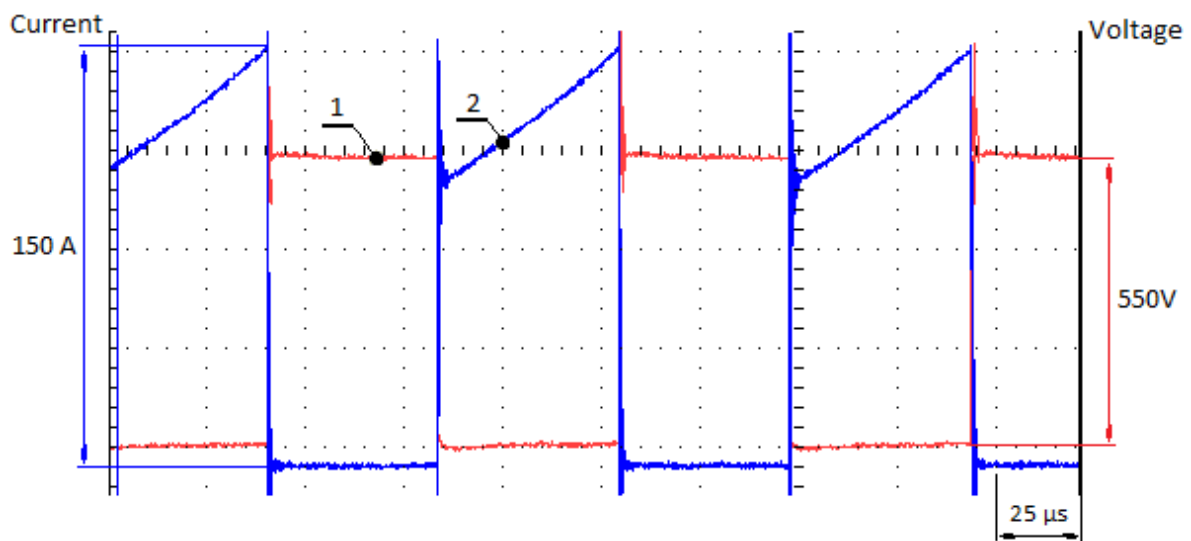


Figure 11. Buck mode of operation. 1 – voltage gate-to-source Q1 (module M1, figure 2), 2 – current through transistors Q1. Snubber capacitors are not included

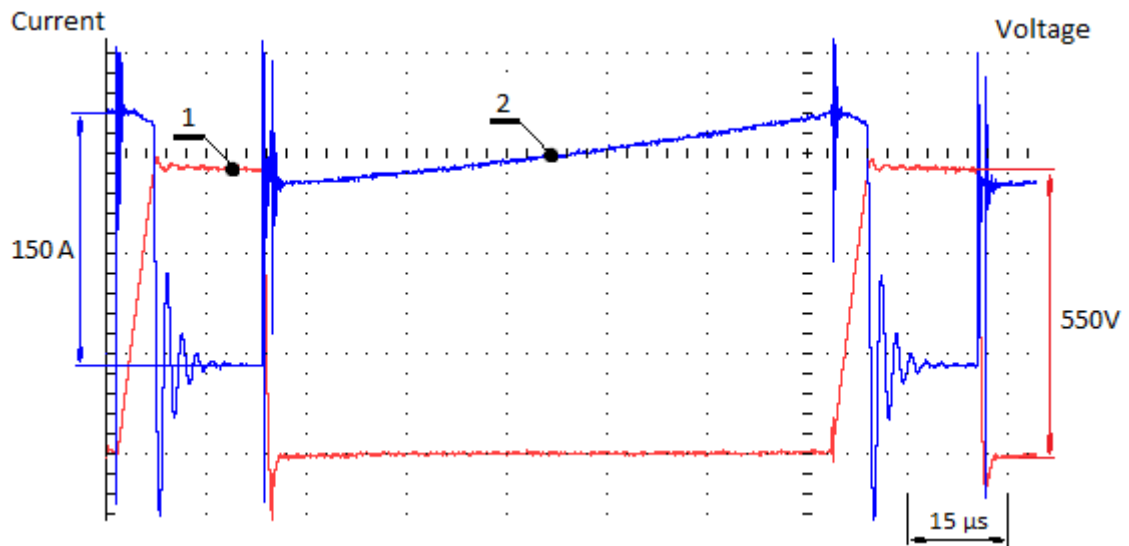


Figure 12. Buck mode of operation. 1 – voltage gate-to-source Q1 (module M1), 2 – current through transistors Q1. Snubber capacitors are included.

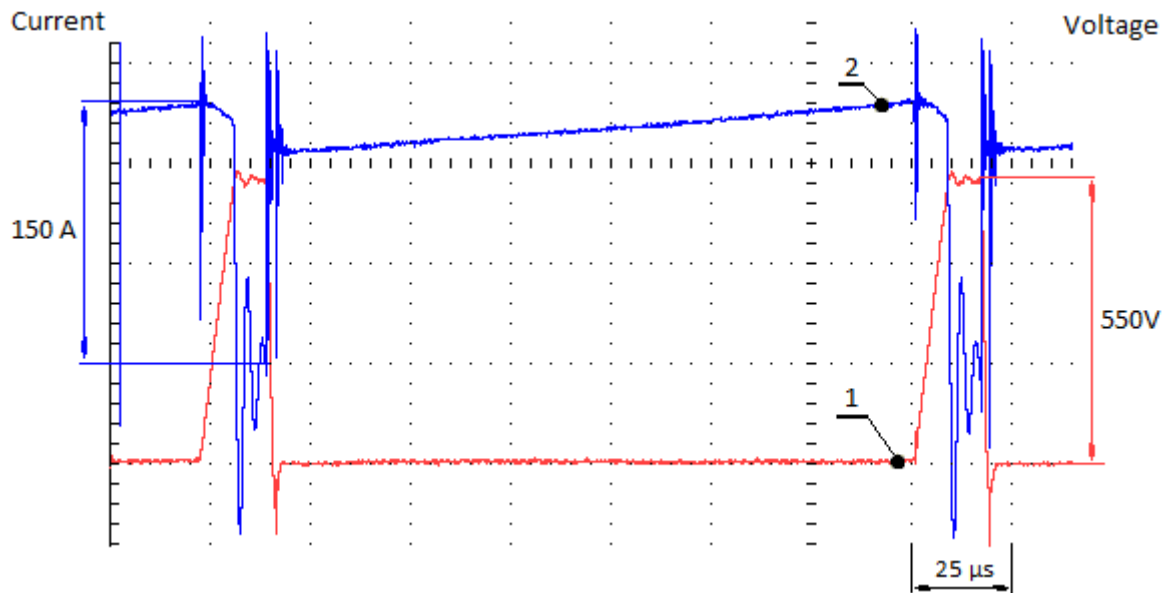


Figure 13. Buck mode of operation. 1 – voltage gate-to-source Q1 (module M1), 2 – current through transistors Q1. Duty cycle over 0.95.

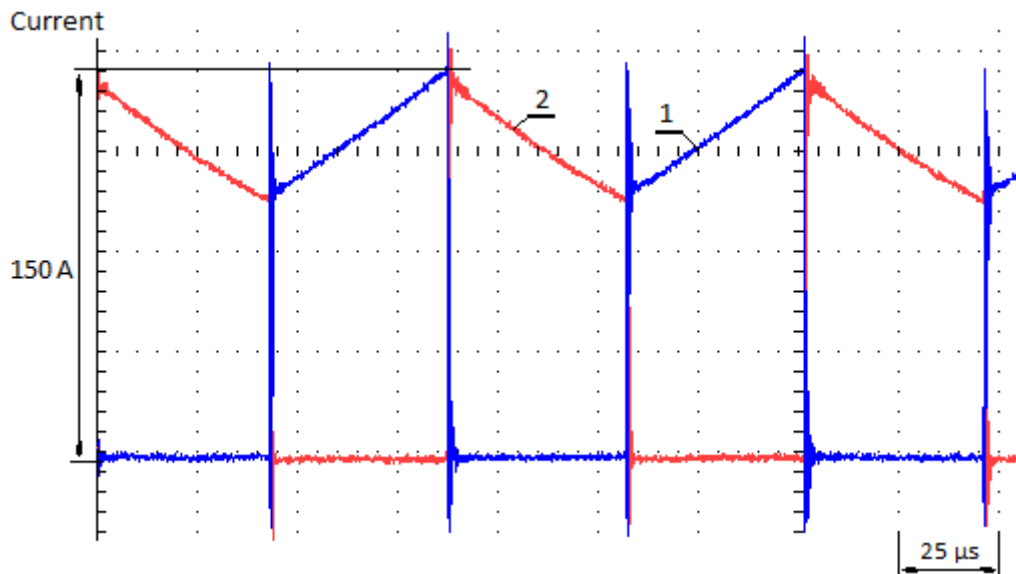


Figure 14. Buck mode of operation. Current through the inductor during 1 – switched-on and 2 – switched-off of transistor Q1.

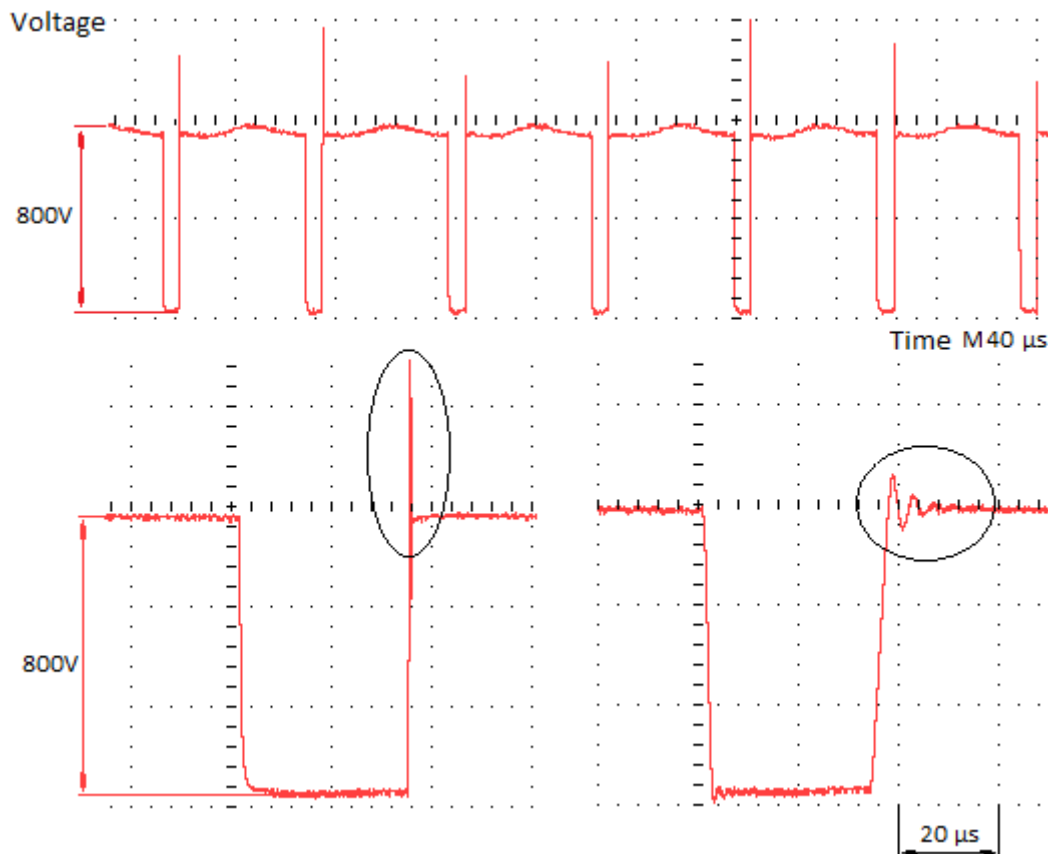


Figure 15. Boost mode of operation. Voltage drain-to-source, boost transistors Q2, module M2.

- Figure 15 shows the Boost mode of operation, drain-to-source voltage of the Boost transistor Q2, M2. The oscillograms in the same figure give the overvoltage of the Boost transistor and its mitigation with the same type of snubber capacitor, connected in parallel to Q2. At the maximum accepted output voltage of 1000V, the peak voltage can potentially exceed the rated voltage of the module of 1200V. Having the same considerations as presented for the Buck

operation mode, it can be stated that the minimum duty cycle, hence the input Boost voltage, must be limited as it is given in figure 4.

- Figure 16. Graphic 1 shows the current through the Boost transistor Q2 (switched-on) and graphic 2 – the current through the diode D2, during the switched-off period of Q2. This measurement verifies the operation of the inductor L1, figure 2, without saturation.
- Figure 17. The voltage (graphic 1) and the current (graphic 2) on the Buck side, i.e. at the input, during the Boost mode of operation is presented.
- Figure 18. The Buck-Boost mode is depicted with the necessary PWM signals only, as all voltages and currents have similar waveforms as already presented for the previous two modes. Herein, Q1 is fixed at 0.8 PWM, graphic 1, and Q2 is variable in the permitted range 0.1 – 0.4 PWM.

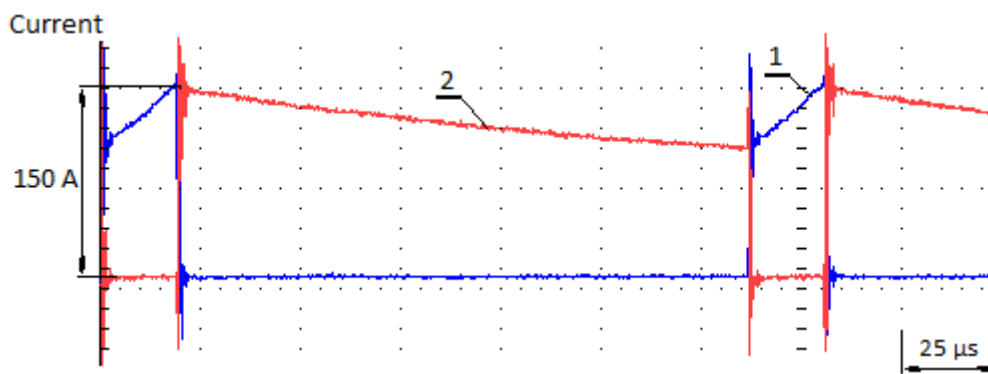


Figure 16. Boost mode of operation. 1 – current through the Boost transistor Q1; 2 – current through the diode D2.

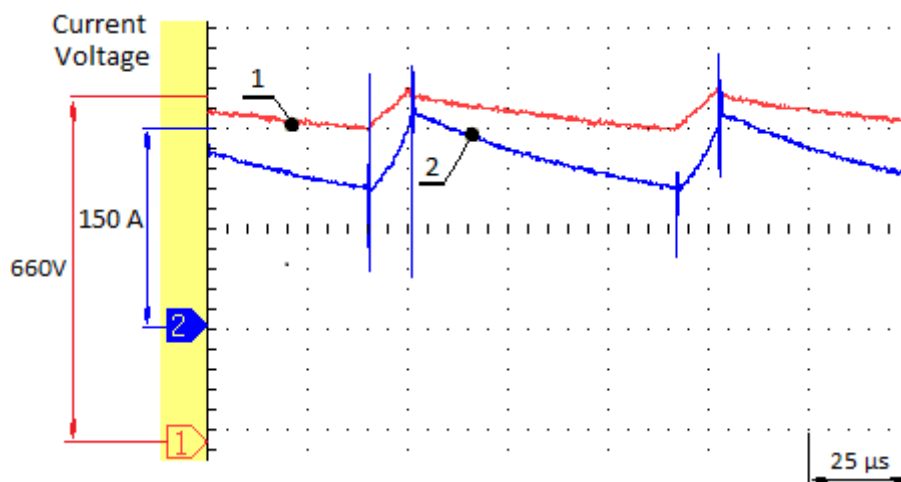


Figure 17. Boost mode of operation. 1 – drain-to-source voltage, Buck transistor Q1, and 2 – current through the transistor Q2 during Boost mode of operation.

- Figure 19. A comparison between the analytically estimated efficiency (1, 3) and experimental measurements (2, 3) is presented. This result shows that the energy analysis given in fig. 7 – fig. 10 can be assumed as valid with an acceptable error under 5%.
- Figure 20. Experimental verification of the expected temperature (2) according to the analytical calculations given in fig. 8 and experimental measurements (1) is presented. The result confirms that the concept of frequency reduction during the Buck-Boost operation mode in order the loses

to be minimized and consequently temperature to be kept under the critical for the ITGT module is valid.

- Figure 21. Comparison between analytically (1, 3) and experimentally (2, 4) estimated power losses, respectively at 12kHz switching frequency and with frequency reduction to 10kHz. The experimentally obtained results are compared according to the analytical data from figure 10.

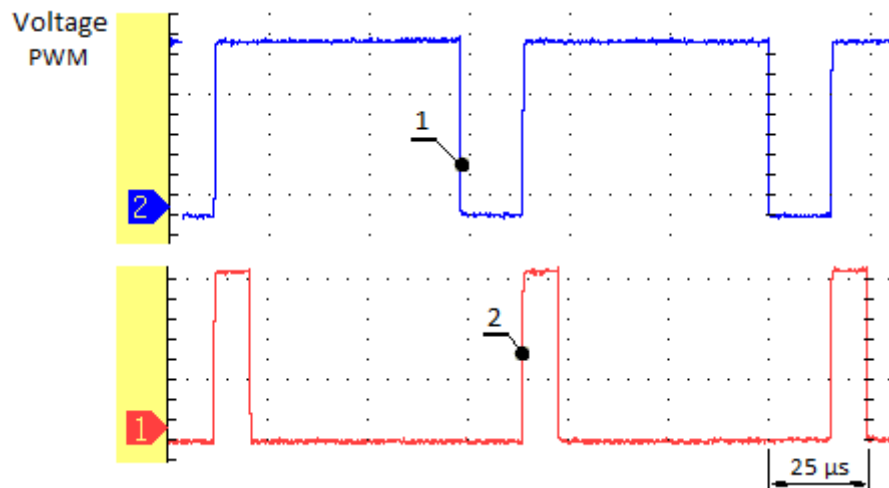


Figure 18. Buck-Boost mode of operation. 1 – PWM on the Buck side, transistor Q1; 2 – PWM on the Boost side – transistor Q2.

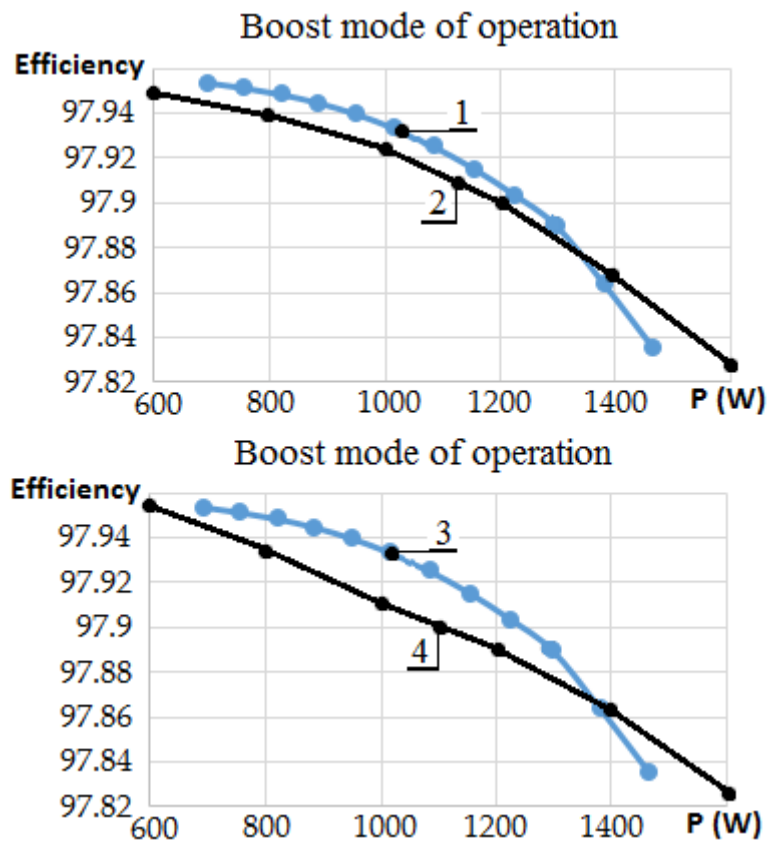


Figure 19. Comparison between analytically 1 and 3, and experimentally 2 and 4 estimated efficiency, according to figure 7 and figure 9.

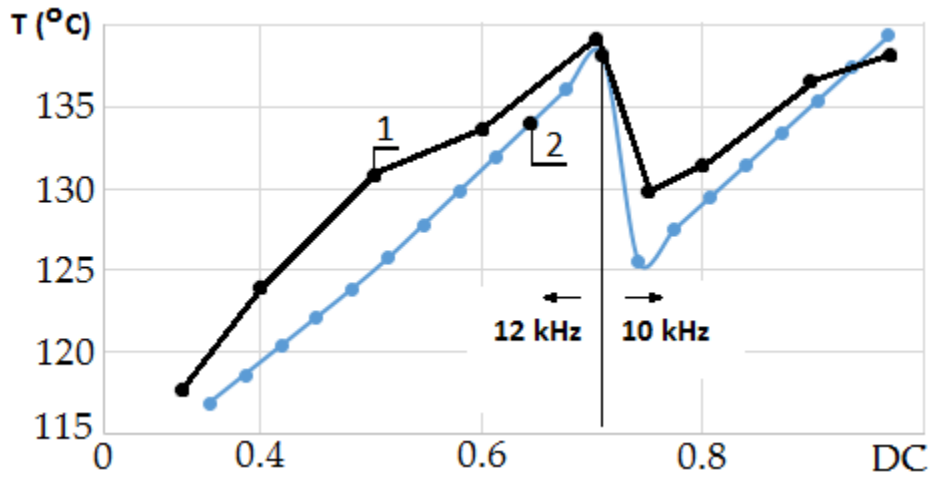


Figure 20. Comparison between analytically (2) and experimentally (1) estimated temperature, according to figure 8.

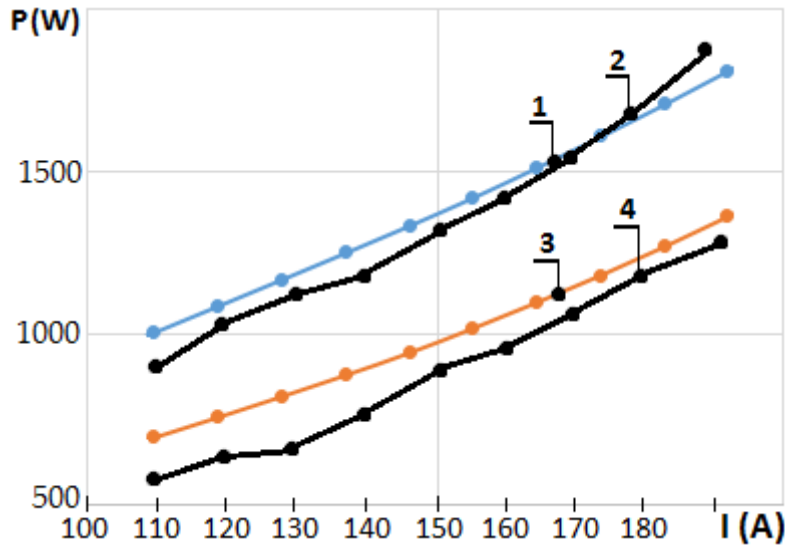


Figure 21. Comparison between analytically (1, 3) and experimentally (2, 4) estimated power losses, respectively at 12kHz and 10kHz, according to figure 10.

3. Conclusions.

In this paper, a buck-boost transformer-less DC-DC converter based on high-voltage IGBT modules for usage in battery charger has been proposed, analyzed and experimentally verified.

The results explicitly showed that a Buck-Boost converter, based on IGBT modules is a possible engineering solution, offering high simple construction, high efficiency, wide output voltage range, which can be lower (step-down) or higher (step-up) than the input DC voltage. By adding an additional module, it can replace the commonly used Buck converter, shown in figure 1., which operates only as a step-down converter. A converter based on IGBTs can be comprised of two transistor-diode modules, as figure 2 shows, or two half-bridge modules given in figure 3, from the currently popular silicon-based semiconductors presented in table 1 (applications).

The presented energy analysis showed that the converter can operate with acceptable power losses and stable thermal operation during the three modes: Buck (figure 7), Boost (figure 9) and Buck-Boost (10). The last one requires the switching frequency to be reduced in order for equalization of the power losses, and hence the junction temperature (figure 8, graphic 4), to be

achieved for the entire voltage range suggested in figure 4. It has been found that the suitable switching frequency for this class hard-switched converters, considering the required power and IGBTs parameters, is around 12kHz, reduced to 10kHz in Buck-Boost operation mode.

The experimental data, presented in figures 11-21, shows that the presented concept can be realized with IGBT modules comprised of transistor-diode structures at the required power. The converter operates stably for the entire range of switching frequencies, which is depicted with oscillograms in figures 11-17. The suggested control conception according to which the switching frequency must be reduced during Buck-Boost mode of operation in order for the temperature to be kept under the maximum junction temperature with a safety margin is verified experimentally, figures 19-21.

Although the presented research is limited to the power part of the suggested converter, the analysis and experimental verification show that a powerful Buck-Boost converter for battery charging, based on a minimum number of modules is a possible solution. A flexible frequency switching control has the magnitude to guaranty a thermal equilibrium of the IGBT modules without power reduction during the entire Buck, Boost and Buck-Boost modes.

Acknowledgments: The authors would like to thank the company **Bowman Power, Southampton, the UK** for their kind support during the development of this research.

Appendix A

Table 1. IGBT modules, suitable for the proposed converter.

| Type | Voltage [V] | Current [A] | E _{on} [mJ] | E _{off} [mJ] | E _r [mJ] | R _{th(j-c)} [K/W] |
|-------------------------|-------------|-------------|----------------------|-----------------------|---------------------|----------------------------|
| Semikron [49] | | | | | | |
| SEMiX452GAL126HDs | 1200 | 319 | 35 | 45 | 33 | 0.15 |
| SKM400GB125D | | 300 | 17 | 18 | 16 | 0.05 |
| SKM400GAL126D | | 300 | 29 | 48 | 27 | 0.08 |
| SKM400GAR126D | | | | | | |
| SEMiX302GAL12E4s | | 356 | 30 | 44 | 19 | 0.096 |
| SEMiX302GAR12E4s | | | | | | |
| SKiiP39GB12E4V1 | | 312 | 20 | 49.7 | 30.2 | 0.19 |
| SEMiX503GB126HDs | | 466 | 20 | 44 | 32.5 | 0.08 |
| Infineon [50] | | | | | | |
| FF300R12KS4HOSA1 | 1200 | 300 | 25 | 15 | 15 | 0.064 |
| FF300R12KE3HOSA1 | | 440 | 25 | 44 | 26 | 0.15 |
| FF450R12KT4 | | 450 | 30 | 40 | 35 | 0.11 |
| Mitsubishielectric [51] | | | | | | |
| CM300DX-24T1 | 1200 | 300 | 36 | 29 | 18 | 0.1 |
| CM450DX-24T1 | | 450 | 56.6 | 42 | 23 | 0.08 |
| Fuji electric [52] | | | | | | |
| 2MBI300U4H-120 | 1200 | 300 | 17 | 19 | 10 | 0.08 |
| 2MBI400VD-120-50 | | 400 | 16 | 18 | 17 | 0.045 |
| 1MBI200VA-120L-50 | | 200 | 15 | 22 | 18 | 0.17 |

| Type | Voltage [V] | Current [A] | E _{on} [mJ] | E _{off} [mJ] | E _r [mJ] | R _{th(j-c)} [K/W] |
|-----------------------|-------------|-------------|----------------------|-----------------------|---------------------|----------------------------|
| 1MBI900VXA-120PC-50 | | 900 | 20 | 40 | 15 | 0.03 |
| 1MBI900VXA-120PD-50 | | | | | | |
| Microsemi [53] | | | | | | |
| APTGT200A120G | 1200 | 400 | 20 | 20 | 18 | 0.14 |
| IXYS [54] | | | | | | |
| MIXA225PF1200TSF | | 360 | 20 | 27 | 11.7 | 0.14 |
| MID 300-12A4 | | 330 | 32 | 29 | - | 0.15 |
| MDI 300-12A4 | 1200 | | | | | |
| MID 550-12 A4 | | 460 | 64 | 59 | - | 0.05 |
| MDI 550-12 A4 | | | | | | |

References

1. R. Wolbertus, R. Van den Hoed, Electric Vehicle Fast Charging Needs in Cities and along Corridors, World Electric Vehicle Journal 10, 45, 2019
2. W. Khan, F. Ahmad, M. Alam, Fast EV charging station integration with grid ensuring optimal and quality power exchange, Engineering Science and Technology, an International Journal 22, 143-152, 2019
3. M. Neaimeha, S. Salisbury, G. Hill, P. Blythe, D. Scofield, J. Francfort, Analysing the usage and evidencing the importance of fast chargers for the adoption of battery electric vehicles, Energy Policy 108, 474-486, 2017
4. T. Gnanna, S. Funkea, N. Jakobsson, P. Plotza, F. Sprei, A. Bennehag, Fast charging infrastructure for electric vehicles: Today's situation and future needs, Transportation Research Part D 62, 314-329, 2018.
5. D. Kim, M. Kim, S. Nengroo, C. Kim, H. Kim, LLC Resonant Converter for LEV (Light Electric Vehicle) Fast Chargers, Electronics, 8, 362, 2019
6. X. Yan, J. Li, B. Zhang, Z. Jia, Y. Tian, H. Zeng, Z. Lv, Virtual Synchronous Motor Based-Control of a Three-Phase Electric Vehicle Off-Board Charger for Providing Fast-Charging Service, Applied Science, 8, 856, 2018
7. J. Lia, D. Wang, W. Wang, J. Jiang, Minimize Current Stress of Dual-Active-Bridge DC-DC Converters for Electric Vehicles Based on Lagrange Multipliers Method, Energy Procedia 105, 2733-2738, 2017
8. I. Lee, J. Lee, A High-Power DC-DC Converter Topology for Battery Charging Applications, Energies MDPI, vol. 10(7), 2017.
9. A. Al-Ogaili, I. Aris, R. Verayiah, A. Ramasamy, M. Marsadek, N. Rahmat, Y. Hoon, A. Aljanad, A. Al-Masri. A Three-Level Universal Electric Vehicle Charger Based on Voltage-Oriented Control and Pulse-Width Modulation, Energies 12, 2019
10. S. Khan, K. Mehmood, Z. Haider, S. Bukhari, S. Lee, M. Rafique, C. Kim, Energy Management Scheme for an EV Smart Charger V2G/G2V Application with an EV Power Allocation Technique and Voltage Regulation, Applied Science 8, 648, 2018
11. Perpina, J. Serviere, X. Jorda, A. Fauquet, S. Hidalgo, J. Ibanez, J. Rebollo, M. Guyennet, IGBT module failure analysis in railway applications, Microelectronics Reliability 48, 1427-1431, 2008
12. P. Gorecki, K. Gorecki, Modelling a Switching Process of IGBTs with Influence of Temperature Taken into Account, Energies 12, 2019
13. F. Napoli, A. Magnani, M. Coppola, P. Guerriero, V. D'Alessandro, L. Codecasa, P. Tricoli, S. Daliento, On-Line Junction Temperature Monitoring of Switching Devices with Dynamic Compact Thermal Models Extracted with Model Order Reduction, Energies, 10, 189, 2017
14. Y. Chang, W. Li, H. Luo, X. He, F. Iannuzzo, F. Blaabjerg, W. Lin, A 3D Thermal Network Model for Monitoring Imbalanced Thermal Distribution of Press-Pack IGBT Modules in MMC-HVDC Applications, Energies 12, 1319, 2019.
15. A. Lucas, G. Trentadue, H. Scholz, M. Otura, Power Quality Performance of Fast-Charging under Extreme Temperature Conditions, Energies 11, 2635, 2018
16. R. Hocine, S. Pulko, A. Stambouli, A. Saidane, TLM method for thermal investigation of IGBT modules in PWM mode, Microelectronic Engineering 86, 2053-2062, 2009

17. N. An, M. Du, Z. Hu, K. Wei, A High-Precision Adaptive Thermal Network Model for Monitoring of Temperature Variations in Insulated Gate Bipolar Transistor (IGBT) Modules, *Energies* 11, 595, 2018
18. E. Jung, Y. Cho, E. Kang, Y. Kim, M. Sung, A Study on the Design and Electrical Characteristics Enhancement of the Floating Island IGBT with Low On-Resistance, *Journal of Electrical Engineering & Technology* Vol. 7, No. 4, pp. 601-605, 2012
19. X. Huang, D. Chang, C. Ling, T. Zheng, Research on Single-Phase PWM Converter with Reverse Conducting IGBT Based on Loss Threshold Desaturation Control, *Energies* 10, 1845, 2017
20. X. Huang, C. Ling, D. Chang, X. You, T. Zheng, Loss Characteristics of 6.5 kV RC-IGBT Applied to a Traction Converter, *Energies* 10, 891, 2017
21. A. Benmansour, S. Azzopardi, J. Martin, E. Woïrgard, Trench IGBT failure mechanisms evolution with temperature and gate resistance under various short-circuit conditions, *Microelectronics Reliability* 47, 1730-1734, 2007
22. A. Benmansour, S. Azzopardi, J.C. Martin, E. Woïrgard, A step by step methodology to analyze the IGBT failure mechanisms under short circuit and turn-off inductive conditions using 2D physically based device simulation, *Microelectronics Reliability* 47, 1800-1805, 2007
23. J. Jeong, S. Hong, S. Park, Field failure mechanism and improvement of EOS failure of integrated IGBT inverter modules, *Microelectronics Reliability* 47, 1795-1799, 2007
24. Y. Belmehdi, S. Azzopardi, A. Benmansour, J. Deletage, E. Woïrgard, Uni-axial mechanical stress effect on Trench Punch through IGBT under short-circuit operation, *Microelectronics Reliability* 49, 1398-1403, 2009
25. J. Urresti-Ibanez, A. Castellazzi, M. Piton, J. Rebollo, M. Mermet-Guyennet, M. Ciappa, Robustness test and failure analysis of IGBT modules during turn-off, *Microelectronics Reliability* 47, 1725-1729, 2007
26. G. Busatto, C. Abbate, B. Abbate, F. Iannuzzo, IGBT modules robustness during turn-off commutation, *Microelectronics Reliability* 48, 1435-1439, 2008
27. L. Chen, J. Xu, S. Cheng, L. Liu, L. Deng, Stability analysis and AC modeling of high-efficiency Buck/Boost converter. 2008 IEEE International Conference on Electron Devices and Solid-State Circuits, 8-10 Dec. 2008
28. X. Ren, X. Ruan, H. Qian, M. Li, Q. Chen, Dual-Edge Modulated Four-Switch Buck-Boost Converter, *IEEE Power Electronics Specialists Conference* 2008
29. C. Wei, C. Chen, K. Wu, I. Ko, Design of an Average-Current-Mode Noninverting Buck-Boost DC-DC Converter with Reduced Switching and Conduction Losses, *IEEE Transactions on power electronics*, Vol. 27, No. 12, December 2012
30. R. Lin, R. Wang, Non-inverting Buck-Boost Power-Factor-Correction Converter with Wide Input-Voltage-Range Applications, *IECON 2010 - 36th Annual Conference on IEEE Industrial Electronics Society*, 2010
31. F. Zhang, J. Xu, P. Yang, Z. Chen, Single-Phase Two-Switch PCCM Buck-Boost PFC Converter with Fast Dynamic Response for Universal Input Voltage, 8th International Conference on Power Electronics - ECCE Asia, The Shilla Jeju, Korea May 30-June 3, 2011
32. X. Ren, Z. Tang, X. Ruan, J. Wei, G. Hua, Four Switch Buck-Boost Converter for Telecom DC-DC Power Supply Applications, *Twenty-Third Annual IEEE Applied Power Electronics Conference and Exposition* 2008
33. D. Denning, A buck-or-boost converter module with embedded inductor and fast current limit, *IEEE Transactions on power electronics*, vol. 26, No. 12, December 2011
34. J. Shiao, C. Cheng, Design of a non-inverting synchronous Buck-Boost DC/DC power converter with moderate power level, *Robotics and Computer-Integrated Manufacturing* 26, 263-267, 2010
35. S. Angkititrakul, H. Hu, and Z. Liang, Active Inductor Current Balancing for Interleaving Multi-Phase Buck-Boost Converter, *Twenty-Fourth Annual IEEE Applied Power Electronics Conference and Exposition* 2009
36. C. Chang, C. Wei, Single-inductor four-switch non-inverting Buck-Boost dc-dc converter, *Proceedings of 2011 International Symposium on VLSI Design, Automation and Test*, 25-28 April 2011
37. Y. Lee, A. Khaligh, A. Chakraborty, A. Emadi, Digital Combination of Buck and Boost Converters to Control a Positive Buck-Boost Converter and Improve the Output Transients, *IEEE Transactions on power electronics*, vol. 24, No. 5, May 2009
38. Application note AN4449, Buck-boost converter using the STM32F334 Discovery kit, STMicroelectronics, 2014. (accessed 8/Jan /2020, https://www.st.com/resource/en/application_note/dm00108726.pdf)

39. Application note TND6253/D, Gate Driver Design Considerations for 4-Switch Buck-Boost Converters, Semiconductor Components Industries, LLC, 2018 (accessed 8/Jan/2020, <https://www.onsemi.com/pub/Collateral/TND6253-D.pdf>)
40. Application Note SLVA535A, Design Calculations for Buck-Boost Converters, Texas Instruments 2012 (accessed 8/Jan/2020, www.ti.com/lit/an/slva535b/slva535b.pdf)
41. Application Note: PMP21529, 4-Switch Buck-Boost Bi-directional DC-DC Converter Reference Design, (accessed 8/Jan/2020, www.ti.com/lit/ug/tidt046/tidt046.pdf)
42. Pressman A., Switching Power Supply Design, ISBN 0-07-052236-7, second edition 1998
43. Billings K., T. Morey, Switch Mode Power Supply Handbook. ISBN: 978-0-07-163972-9, third edition 2011
44. IGBT Application Note, R07AN0001EJ0410, Renesas Electronics, Rev.4.10, (accessed 8/Jan/2020, https://www.renesas.com/en-us/doc/products/igbt/apn/r07an0001ej0410_igbt.pdf)
45. A. Wintrich, U. Nicolai, W. Tursky, T. Reimann, Application Manual Power Semiconductors, SEMIKRON International 2015 (accessed 8/Jan/2020, <https://www.semikron.com/dl/service-support/downloads/download/semikron-application-manual-power-semiconductors-english-en-2015.pdf>)
46. B. Baliga, The IGBT Device Physics, Design and Applications of the Insulated Gate Bipolar Transistor, ISBN: 978-1-4557-3143-5, Elsevier Inc. 2015
47. A. Volke, M. Hornkamp, IGBT Modules, Technology, Driver and Application, Infineon Technologies AG, ISBN 978-3-00-040134-3, Second Edition 2012
48. V. Khanna, The Insulated Gate Bipolar Transistor IGBT Theory and Design, Wiley-Interscience, ISBN 0-471-23845-7, 2003
49. <https://www.semikron.com/> (accessed 8/Jan/2020)
50. <https://www.infineon.com/> (accessed 8/Jan/2020)
51. <http://www.mitsubishielectric.com/> (accessed 8/Jan/2020)
52. <https://www.fujielectric.com/> (accessed 8/Jan/2020)
53. <https://www.microsemi.com/> (accessed 8/Jan/2020)
54. <http://www.ixys.com/> (accessed 8/Jan/2020)